Multidisciplinary Design Analysis and Optimisation of Rear Wings for Sports Cars

Miguel da Silva Ferreira
miguel.s.ferreira@ist.utl.pt

Instituto Superior Técnico, Lisboa, Portugal

June 2016

Abstract

Rear wings are aerodynamic devices that highly influence the performance of a vehicle. This work deals with an aero-structural optimisation problem of such devices, where the multiphysics involved was considered by means of fluid-structure interaction (FSI) towards effective and safe designs, for minimum drag and mass. The objective is to fold the implementation of a process for optimal automotive aerodynamic devices design. Two study cases were considered: a traditional rear wing design used in both automotive and motorsport applications; and a proposed design, where the surface connection between the endplates and vertical supports is used to create additional downforce. A multidisciplinary design analysis and optimisation (MDAO) framework was defined through a computer-aided engineering (CAE) software (ANSYS® Workbench 14.5). Optimal designs results were achieved from multidisciplinary parametric and optimisation analyses. The present work showed that the process employed is very well suited for the preliminary design phase of aerodynamic devices in producing efficient products in a relative short time frame. Mesh and turbulence modelling strategy proved to be important regarding the accuracy of the numerical solutions and for problems with small deformations, a FSI one-way coupling technique has significant computational advantages.

Keywords: Aero-structural problem, Fluid-structure interaction, Computer-aided engineering, Aerodynamic devices, Composite materials.

1. Introduction

In the late 1960s, several teams in motorsport started to use rear wings in their race cars and it was at this point that aerodynamics began to play a key role in high-performance cars design [3]. Combined with engines innovations, speeds increased significantly and the wings structural integrity became an important consideration. The 1980s marked the beginning of composite materials use in the automotive industry and until today, aerodynamicists and engineers focus in achieving the best possible aerodynamic efficiency (maximum downforce, minimum drag) for the lightest vehicles. Due to their high strength-to-weight ratio, the use of these materials has increased significantly in the automotive industry, as well as in other branches of engineering [7].

Rear wings have an essential function in the exploitation of downforce and when designing them, the prevailing three-dimensional flow caused by the presence of the vehicle's body and its different components should be known. The fine tuning of designing a rear wing is therefore unique to each vehicle. The biggest downside is that proper computational or experimental tools are required and because of that, in this work, wings were designed considering free-flow conditions only. Besides this, in order to achieve effective and safe designs, it is crucial to consider the multiphysics involved, especially if aero-elastic phenomena are expected. Usually aerodynamic devices experience small deformations and the fluid-structure interaction (FSI) can be treated as an aero-structural problem [4]. To efficiently couple the aerodynamic and structural disciplines and achieve optimised solutions, a multidisciplinary design analysis and optimisation (MDAO) framework was defined for specific design variables and objective functions.

The main objective of this work was to fold the implementation of a process for optimal automotive aerodynamic devices design, through two different rear wings configurations: a traditional one, commonly used in high-performance cars, and a proposed design, where the surface connection between the endplates and vertical supports is used to create additional downforce. The design will be comprised of two main steps: verify and choose appropriate settings for the disciplinary modules (methodology)

and define the MDAO process for the FSI system, to obtain minimum drag, structural deformation and mass. Figure 1 describes the overall scheme of the MDAO system established for the aero-structural optimisation problem of this work.

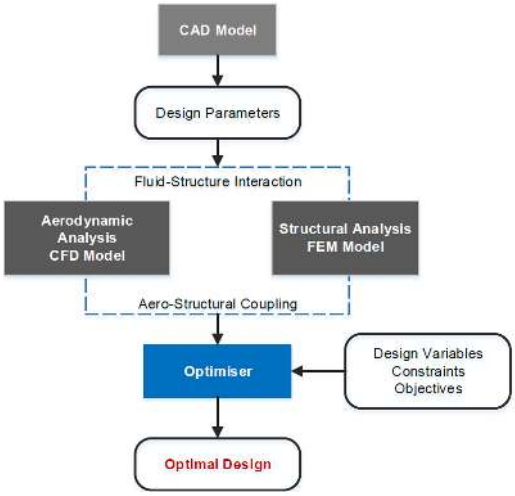

Figure 1: MDAO framework established for the aero-structural optimisation problem.

2. Theoretical Background

FSI is a combination of fluid and structural dynamics, both described by the relations of continuum mechanics and solved with numerical models. Therefore the aerodynamic and thin structures fundamental theory, as well as the MDAO purpose along with different optimisation methods are briefly covered in this section.

2.1. Aerodynamic Theory

The solution of the fluid flow is based on the *Reynolds-averaged Navier Stokes equations* (RANS) given by [12]:

$$\frac{\partial \overline{u_i}}{\partial x_i} = 0\,, \tag{1}$$

$$\frac{\partial \overline{u_i}}{\partial t} + \overline{u_j}\frac{\partial \overline{u_i}}{\partial x_j} = \overline{f_i} - \frac{1}{\rho}\frac{\partial \overline{p}}{\partial x_i} + \nu\frac{\partial^2 \overline{u_i}}{\partial x_j \partial x_j} - \frac{\partial \overline{u_i' u_j'}}{\partial x_j}\,, \tag{2}$$

where the solution variables (ϕ), fluid density (ρ), components of the fluid velocity (u_i), external forces (f_i), fluid pressure (p) and fluid kinematic viscosity (ν) are split into mean and fluctuation values: $\phi = \overline{\phi} + \phi'$. In this equation, $\overline{u_i' u_j'}$ is the Reynolds stress tensor which is calculated with turbulence models.

Turbulent flows are significantly affected by the presence of walls. The no-slip condition at the wall must be satisfied and a boundary layer is generated. Numerous experiments have shown that the near-wall region can be subdivided into three regions [12]: the *viscous sublayer*, *buffer layer* and *log-law region*. In the fluid flow direction, x-axis, the dimensionless wall distance is defined as $y^+ = \frac{y\,u_\tau}{\nu}$ where u_τ is the friction velocity and y is the height of the first cell. The success of RANS models is essentially established by the efficiency and accuracy in the computation of wall-bounded flows, which can be evaluated by the y^+ values [5].

The k-ϵ and k-ω two-equation models or the γ-$Re_{\theta t}$ four-equation model are some of the most used in automotive aerodynamics for CFD simulations [4].

The k-ϵ models are used in combination with wall functions and the each wall adjacent cells should be located within the log-low region ($30 < y^+ < 500$). The k-ω turbulence model is considered to be more suitable for complex boundary layer flows and it uses the near-wall formulation ($y^+ < 5$) [6]. One of the major drawbacks of the two-equation turbulence models is that they model the flow as fully turbulent. To accurately predict the onset of transition and describe both laminar and turbulent regimes, the γ-$Re_{\theta t}$ transition model solves two additional transport equations based on experimental correlations (also advised to have $y^+ < 5$) [6].

2.2. Structures Theory

The calculations for the structure side are based on the impulse conservation [1], solved by a finite element approach described as

$$\mathrm{M}\cdot\ddot{\vec{u}} + \mathrm{C}\cdot\dot{\vec{u}} + \mathrm{K}\cdot\vec{u} = \vec{F}\,, \tag{3}$$

where M is the *global mass matrix*, C the *global damping matrix*, K the *global stiffness matrix*, $\vec{F}$ is the vector of external forces and $\ddot{\vec{u}}$, $\dot{\vec{u}}$ and $\vec{u}$ are the nodal acceleration, velocity and displacements vectors, respectively. For static analysis this equation becomes simply $\mathrm{K}\cdot\vec{u} = \vec{F}$.

This work deals not only with isotropic linear elastic materials, governed by the generalised *Hooke's law*, but also with fiber-reinforced laminated anisothropic materials, such as carbon fibres. In the analysis of layered composite structures, shell elements are widely used to keep the computational effort reasonable. In-plane stresses and transverse shear stresses can be predicted with good accuracy using shells based on the *First-Order Shear Deformation* theory (FSDT) [7].

2.3. Fluid-Structure Interaction

The solution strategies for FSI numerical simulations are mainly divided into two distinctive methods: the *monolithic method* and the *partitioned method* [1]. In the monolithic method (also called *fully coupled*), fluid and structure dynamics sides are formulated as one combined problem, where equations are solved together. It requires a fully integrated FSI solver which is computationally expensive.

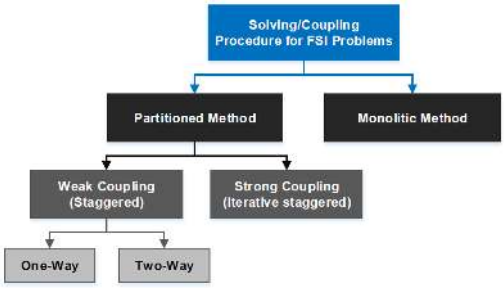

Figure 2: Solution strategies for FSI problems.

Nowadays, a common way to deal with FSI applications is to use partitioned methods. By allowing to reuse existing efficient CFD and computational structural mechanics (CSM) software separately, where interaction effects are treated as boundary conditions at the fluid-solid interface, software modularity is preserved and FSI problems can be solved faster when compared to the monolithic method [4, 11]. Furthermore, the partitioned method can be categorised into two different types of coupling algorithms: weakly coupled (or *staggered*) and strongly coupled (or *iterative staggered*). Weak coupling can be further divided between one-way coupling, where only the fluid pressure acting at the structure is transferred to the structural solver, or two-way coupling, where the displacements of the structure are also transferred to the fluid solver. An overview of the different solving procedures for FSI problems can be seen in Fig. 2.

This work will deal only with weak coupling strategies, and for those interested in the differences between strong and weak coupling methods can find information in [11].

2.4. Multidisciplinary Design Analysis and Optimisation

Besides achieving an optimal design of products that involve more than one field of expertise, the aim of MDAO is to accomplish the optimisation process efficiently (in the shortest time possible). There are different MDAO strategies that can be more appropriate according to the design problem. Considerable research has already been performed on the advantages and disadvantages of particular MDAO strategies, both in the automotive [9] and aerospace applications [10]. The purpose of this project is not to fully delve into this, however, issues concerning MDAO will appear during the course of this work.

2.5. Numerical Optimisation Techniques

Optimisation problems are solved using algorithms that consist of an iterative search process. There are various methods that can be used and its suitability depends on the nature of the problem. These methods could range from direct methods (gradient based local solvers and non-gradient global based methods), to indirect methods (using response surface techniques). Gradient based methods are considered to be fast and require relatively small number of design point evaluations to reach local optimum [9].

3. Methodology

In order to accomplish the objectives proposed for this work, taking into account the computational resources available and the synergy of the different complex disciplines involved, a *Computer-Aided Endineering* (CAE) software was used, the ANSYS® Workbench 14.5.

In this section, description of ANSYS® numerical models utilised to perform the rear wings multidisciplinary analyses are presented. The focus was to define the specific modelling techniques and settings to be adopted regarding both reliability and quality of the numerical solutions of this work.

3.1. CAD Model: ANSYS® DesignModeler

To bypass geometries importation with further *Computer-Aided Design* (CAD) corrections, the ANSYS® *DesignModeler* software was used to create all the geometries of this work (example in Fig. 3). It also had parametric capabilities, important in defining the design variables of interest for the MDAO process.

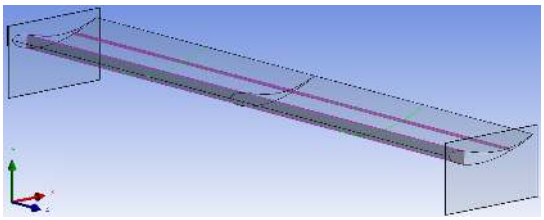

Figure 3: Wing geometry used in CFD and CSM studies.

3.2. CFD Model: ANSYS® Fluent

The quality of CFD numerical solutions strongly depends on user-defined elements such as the mesh generation and turbulence modelling. Concerning the reliability of the CFD solutions presented in this work, investigations were conducted for two-dimensional NACA 4415 airfoil and validated against data from [2]. The closeness of the comparison between *Fluent* results and the experimental data gave an acceptable level of confidence in the accuracy of further three-dimensional numerical simulations.

Double-precision, steady-state and *pressure-based* algorithm were the solver settings defined for the CFD simulations presented in this work, as advised by [5] to compute the flow around both au-

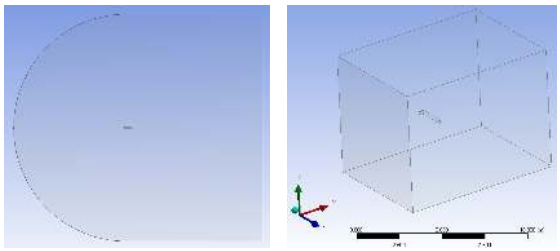

(a) Two-dimensional studies (blockage ratio of 1.2%). (b) Three-dimensional studies (blockage ratio of 1%).

Figure 4: Virtual wind tunnel geometries for the aerodynamic studies of this section.

Table 2: Turbulence modelling influence (comparison to experimental data).

Model	y^+	ΔC_l %	ΔC_d %	ΔC_m %
γ-$Re_{\theta t}$	0.1/1.8	−0.40	−1.52	−2.53
k-ω SST	0.2/1.9	−9.88	+71.89	−14.69
Realizable k-ϵ	19.1/312.8	−11.89	+45.79	−39.56

tomobiles and wings. With respect to the solution methods, the pressure-velocity coupling scheme selected was the *semi-implicit method for pressure-linked equations* (SIMPLE). Spatial discretisation schemes were defined to *least squares cell based* for the gradient, *standard* for the pressure and *second order upwind* for the momentum and turbulent kinematic energy and dissipation rate. The solution control was made by monitoring the convergence of residuals statistics and lift, drag and moment coefficients values (C_l, C_d and C_m respectively).

Virtual wind tunnel dimensions are important to disregard blockage effects (advised by [3] to have blockage ratio values lower than 5%). Following recommendations of [5], the boundary conditions for the virtual wind tunnel geometry (Fig. 4(a)) were defined as: *velocity inlet* (left side), *pressure outlet* (right side), *symmetry* (for the upper and lower sides) and *wall* with no-slip condition for the airfoil walls.

An hybrid mesh strategy has been employed in the CFD analyses of this work. Both generation of the structured prismatic layers and airfoil number of divisions (mesh density), as well as the turbulence modelling strategy (presented in Table 2) were the focus of the two-dimensional analyses.

Overall, the γ-$Re_{\theta t}$ transition model proved to be a much more trustworthy choice when compared to the two-equation turbulence models realizable k-ϵ and k-ω SST. By ensuring that the prismatic layers were within the structured mesh zone, notable improvements in the accuracy of the numerical solutions were observed.

The γ-$Re_{\theta t}$ model in Table 2 (test case 'XXIV') was applied and considered as the role model to further 50 m/s flow velocity three-dimensional CFD analyses (designated as test case 'I'), where the wing geometry considered was the one of Fig. 3, and the aerodynamic performance was assessed for downforce ($-L$), drag (D) and wing efficiency ($-L/D$) values. Same strategy for the virtual wind tunnel dimensions from two-dimensional analyses was used (Fig. 4(b)).

The influence of the mesh density in the solution accuracy was investigated and the coarser meshes produced reasonable results when compared to the fine meshes, as seen in Table 1.

From the parametric studies performed in Section 4, the γ-$Re_{\theta t}$ model proved to be extremely dependent on the inlet flow conditions when solving low-Reynolds numbers simulations. *Fluent* struggled in obtaining reliable results with non-converged solutions. In order to overcome this and improve the overall mesh quality, further three-dimensional studies were conducted. By disregarding prismatic layers generation, the realizable k-ϵ model in combination with non-equilibrium wall functions was evaluated and good results were obtained with stable and fast converging solutions compared to the γ-$Re_{\theta t}$ model. This specific turbulence model is widely used in academic and industrial automotive applications [4, 5].

Based on these analyses, succeeding rear wings aerodynamic parametric studies are presented for 50 m/s flow velocity with both model application of test cases 'IV Opt.' (γ-$Re_{\theta t}$) and 'VI Opt.' (realizable k-ϵ). Optimisation analyses are presented only for the 'VI Opt.' test case model application and final values for the test case 'II'.

Table 1: Three-dimensional fluid flow studies with *Fluent* for different turbulence modelling and meshing strategies. [NE is the total number of elements; Δt is the duration of the analysis, for 1000, 1000, 500 and 500 iterations respectively; Δ is the relative percentage variation calculated in relation to the first 'I (γ-$Re_{\theta t}$)' test case.]

Test case (Model)	NE	Δt	$-L\,(N)$	Δ %	$D\,(N)$	Δ %	$-L/D$	Δ %
I (γ-$Re_{\theta t}$)	6 699 559	8 h	938.8	—	59.1	—	15.89	—
IV Opt. (γ-$Re_{\theta t}$)	1 805 605	3 h	913.5	−2.70	58.2	−1.47	15.69	−1.25
II (realizable k-ϵ)	2 887 477	45 min	929.1	−1.03	61.9	+4.77	15.00	−5.55
VI Opt. (realizable k-ϵ)	1 445 577	20 min	953.9	+1.61	64.4	+8.95	14.82	−6.74

Table 3: Three-dimensional wing mesh sensitivity investigations with *ACP* and *Mechanical* for *SHELL181* and *SHELL281* elements with one-way FSI coupling technique. [CSM Imported Loads transfer relative errors (ΔD % and ΔL %) are calculated in relation to the CFD results (D: 59.0 N and L: −940.1 N); maximum deformation values U_{max} relative variations Δ % are calculated in relation to the 'Mesh I' test case results.]

		SHELL181				*SHELL281*			
Test Case	No. of Elements	Imported Loads ΔD %	Imported Loads ΔL %	U_{max} (mm)	Δ %	Imported Loads ΔD %	Imported Loads ΔL %	U_{max} (mm)	Δ %
Mesh VII	481 808	−3.93	+0.01	1.42	+1.29	−3.72	+0.01	1.45	+0.27
Mesh I	288 962	−0.39	+0.11	1.40	—	−2.55	+0.02	1.44	—
Mesh II	145 926	−3.36	+0.01	1.37	−2.08	−3.36	+0.01	1.44	−0.54
Mesh III	73 474	−2.99	−0.02	1.33	−4.94	−2.99	−0.02	1.41	−2.59
Mesh IV	36 504	−1.44	+0.04	1.27	−9.37	−1.01	+0.09	1.38	−4.42
Mesh V	18 738	−2.09	−0.21	1.19	−14.96	+1.52	−0.23	1.34	−7.33
Mesh VI	9 866	+24.14	−0.67	1.11	−20.36	+24.16	−0.66	1.27	−11.83

3.3. CSM Model: ANSYS® Composite PrepPost and Mechanical

In this section, a one-way FSI coupling technique was used to transfer the aerodynamic loads to the CSM model and compute the structural deformations for finite element method evaluation. The aerodynamic loads, mesh generation technique and geometry considered were the same of test case 'I'. Increase in structural stiffness was obtained by using two spars, one located at 20% c and the other one at 70% c from the leading edge (Fig. 3).

The materials considered in the structural parametric studies are based in the ones used in automotive wings, such as isotropic materials (aluminium alloy and ABS Plastic) and orthotropic carbon fibre-reinforced thermoplastics (CFRTP).

When importing loads from *Fluent*, *Mechanical* nodal values are calculated by linear interpolation from the surrounding CFD nodes (thus the mapping process is not conservative) [4]. Therefore the mesh density was investigated in order to understand how important it is necessary to have a matching mesh for FSI applications and its influence in the imported load transfer and solution convergence. Both linear shell elements (*SHELL181*) and quadratic shell elements (*SHELL281*) were considered. Results are presented in Table 3.

The use of *SHELL281* elements demonstrated reliable (safer, as it over-predicted *SHELL181*), faster convergence results for a slight processing time increase. No relevant differences were found in the *Mechanical* computed aerodynamic forces and the coarser the mesh, the smaller the maximum deformation values. As such, the succeeding rear wings structural parametric studies and composite stacking sequence optimisations use the coincident mesh approach (test case 'Mesh I'), following recommendations from [1, 4], using *SHELL281* type elements, where the computed CFD aerodynamic loads were considered for a 90 m/s flow velocity.

3.4. FSI Model: ANSYS® System Coupling

There are two different approaches to solve FSI problems in ANSYS® Workbench: a straightforward technique for one-way coupling (used in the previous CSM analyses) and for a fully coupled iterative solution at each time step, using the *System Coupling* to perform both one-way and two-way analyses. A simple non-qualitative problem was conducted in order to understand and evaluate the computational efficiency in resources when using each of these techniques to establish the FSI procedure for the following structural parametric and optimisation studies.

Such non-qualitative sub-study was done for a simple flat plate geometry exposed to wind flow, where the mesh strategy was the same of the previous structural analyses of Subsection 3.3. Based on the results presented in Table 4, the use of the *System Coupling* to solve FSI problems proved to be extremely computationally expensive.

Considering that the rear wings deformations will be small, the FSI technique used for the structural parametric and optimisation analyses was the straightforward one-way coupling technique.

Table 4: Approximate values of the processing time when performing FSI analyses using different FSI coupling techniques for the plate exposed to wind flow test case.

FSI technique	Processing time
One-way FSI	8 *min*
One-way FSI with *System Coupling*	40 *min*
Two-way FSI with *System Coupling*	1 *h* 30 *min*

3.5. Optimisation Model: ANSYS® Direct Optimisation

In order to achieve optimal solutions for both aerodynamic and structural disciplines in a relative short time frame, the MDAO strategy employed follows a sequential optimisation method, where each

sub-system has its own local optimiser.

For the rear wings aerodynamic optimisation, the *Non-Linear Programming by Quadratic Lagrangian* (NLPQL) optimiser was used. It is a gradient based single objective optimiser (others output parameters can be defined as constraints) based on quasi-Newton methods and suited for problems with continuous design variables.

The *Mixed-Integer Sequential Quadratic Programming* (MISQP) optimiser was used to optimise the rear wings structures mass, which is a mathematical optimisation algorithm that solves *Mixed-Integer Non-Linear Programming* (MINLP) for discrete or integer design variables.

4. Results

4.1. Design Variables and Functions of Interest

Regarding the aerodynamic discipline, the wing performance is dictated by the outer geometric parameters. Therefore the aerodynamic design variables of interest were the ones of Table 5. The functions of interest defined were drag, downforce and wing efficiency.

The most important structural factor is the strength allied to lightness of the material chosen for the wing. CFRTP materials are extremely advantageous in these situations. Hence, not only different materials performance was assessed (mentioned in Subsection 3.3), as the number and orientation of plies were also the design variables for the structural discipline. The functions of interest were mass, maximum deformation values and failure performance.

4.2. CAD Parametric Design

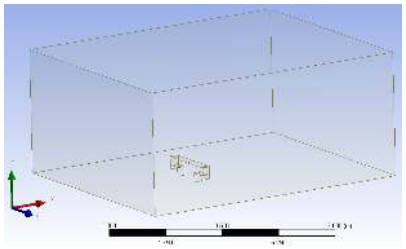

Figure 5: Three-dimensional virtual wind tunnel for the rear wings CFD analyses (blockage ratio of 1.72% for the traditional and 2.59% for the proposed design).

As mentioned in the previous Section 1, in this work, two different design strategies of rear wings were developed, as seen in Fig. 6, according to the values summarised in Table 5. These are comprised of three different components: the wing(s), endplates and vertical supports. *Baseline* aerodynamic performance is given in bold in Table 6.

The wings profile was chosen after research of the most suited for automotive applications, in order to minimise the number of design variables and reduce

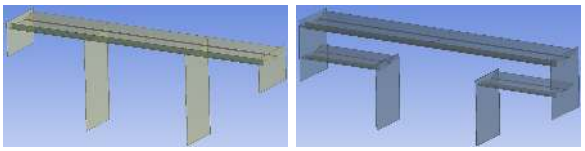

(a) Traditional (TRW). (b) Proposed (PRW).

Figure 6: Baseline parametrised rear wings geometries.

Table 5: Baseline design variables (parameters) values assigned for the rear wings. [LE and TE is the leading edge and trailing edge designation.]

Design variable	Value
Wings angle of attack	1 deg
Wings profile chord	Main wings: 0.30 m Lower wings: 0.25 m
Lower wings position	Horizontal: 0.0 m Vertical: -0.2 m
Main wings half-span	0.9 m
Vertical supports position	0.36 m
Endplates length	5% c (from main wing LE and TE)
Endplates upper distance	5% c (of main wing)
Endplates lower distance	65% c (of main wing)

the computational time to achieve improved designs. A small sub-study (using test case 'I' model application of Section 3) was done for two of the most efficient automotive wing profiles, according to [8], the Benzing BE 122-125 and Eppler 664. From the results presented in Fig. 7, the Benzing BE 122-125 profile was selected to be used in the rear wing designs, much like [8]. It showed better efficiency at lower drag values, for a much greater downforce generation.

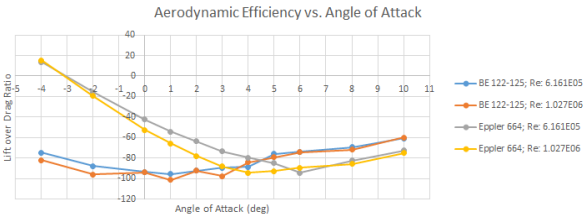

Figure 7: Effect of the angle of attack in the airfoil efficiency.

Both vertical supports and endplates were designed as rectangular plates. In particular, the endplates increases the effective aspect ratio of the wing to achieve efficiency improvements, which was verified by numerical analyses (using test case 'I' model application, $+9.05\%$ $-L/D$). In this work, the vertical supports were rigid and mass disregarded.

For the virtual wind tunnel geometry dimensions, the same approach of Section 3 was used, illustrated in Fig. 5 for the proposed design.

4.3. Aerodynamic Parametric Studies

Prior to investigate the effect of the different design variables common to both rear wings, the proposed design lower wings position was investigated. When moving them to a forward position relative to the main wing, a decrease in efficiency was predicted by both transition and turbulence models considered. This was expected due to the different flow approach characteristics experienced by the wings. The same explanation could be applied to the backward position, yet, the realizable k-ϵ model showed positive effects in the design aerodynamic efficiency. Detailed inspections were conducted using the *CFD-Post* to visualise the flow behaviour of both cases (Fig. 8).

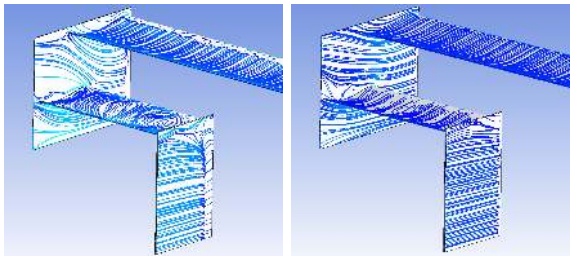

(a) γ-$Re_{\theta t}$ transition model. (b) k-ϵ turbulence model.

Figure 8: Effect of backward position of lower wings (-0.20 m) visualised by surface streamlines.

The k-ϵ model when compared to the γ-$Re_{\theta t}$, predicted a less complex flow behaviour, with much less intense three-dimensional effects. Menter [6] outlined that such behaviours could occur to model complex flows with k-ϵ models and in these situations, transition models are much more reliable. For this reason, the proposed rear wing lower wings horizontal position was fixed for the baseline value of Table 5. For the vertical wings spacing, as expected, increasing this distance produced less intense wings flow interference, which increased the proposed design overall efficiency.

The effect of the two parameters that define the aspect ratio of the wings (profile chord and span) were first investigated. The effect of the main wings chord is presented in Table 6. Overall, increasing the aspect ratio of the wings produced a positive effect in the overall efficiency of the designs, which was in agreement with the literature published by [3]. By reducing the profile chord, greater performance was achieved through greater drag minimisation, whether by increasing the wingspan through greater downforce.

As for the two-dimensional analysis presented in Fig. 7, whether it be increasing the angle of attack of the main wings (Table 6) or lower wings, an increase in downforce was generated with the downside of reducing the overall efficiency. In particular for the proposed design, increasing the angle of attack of the lower wings had critical negative effects on the flow behaviour of the main wing.

For the traditional design, when a vertical support is connected to the wing, it interferes with its boundary layer. The larger the distance between the vertical supports, the larger the wing surface unaffected by the no-slip condition, reducing the drag and promoting a higher pressure difference between the upper and lower wing sides, generating more downforce and improving the overall ef-

Table 6: Rear wings profile chord (PC), angle of attack (AoA) and vertical supports position (PL) effect.

	Traditional rear wing						Proposed rear wing					
PC	$-L\,(N)$		$D\,(N)$		$-L/D\,(N)$		$-L\,(N)$		$D\,(N)$		$-L/D\,(N)$	
(m)	γ-$Re_{\theta t}$	$R.\ k$-ϵ	γ-$Re_{\theta t}$	$R.\ k$-ϵ	γ-$Re_{\theta t}$	$R.\ k$-ϵ	γ-$Re_{\theta t}$	$R.\ k$-ϵ	γ-$Re_{\theta t}$	$R.\ k$-ϵ	γ-$Re_{\theta t}$	$R.\ k$-ϵ
0.25	-13.6%	-14.0%	-21.4%	-21.0%	$+9.8\%$	$+9.0\%$	-7.3%	-6.1%	-16.3%	-14.9%	$+10.8\%$	$+10.4\%$
0.30	**931.7**	**1028.8**	**74.2**	**74.7**	**12.56**	**13.78**	**1289.6**	**1332.1**	**110.3**	**117.9**	**11.69**	**11.30**
0.35	$+14.7\%$	$+13.0\%$	$+21.1\%$	$+21.4\%$	-5.2%	-7.0%	$+7.6\%$	$+6.9\%$	$+17.7\%$	$+16.2\%$	-8.5%	-8.0%
AoA	$-L\,(N)$		$D\,(N)$		$-L/D\,(N)$		$-L\,(N)$		$D\,(N)$		$-L/D\,(N)$	
(deg)	γ-$Re_{\theta t}$	$R.\ k$-ϵ	γ-$Re_{\theta t}$	$R.\ k$-ϵ	γ-$Re_{\theta t}$	$R.\ k$-ϵ	γ-$Re_{\theta t}$	$R.\ k$-ϵ	γ-$Re_{\theta t}$	$R.\ k$-ϵ	γ-$Re_{\theta t}$	$R.\ k$-ϵ
1	**931.7**	**1028.8**	**74.2**	**74.7**	**12.56**	**13.78**	**1289.6**	**1332.1**	**110.3**	**117.9**	**11.69**	**11.30**
5	$+25.4\%$	$+27.6\%$	$+49.3\%$	$+44.4\%$	-16.0%	-11.6%	$+21.9\%$	$+22.1\%$	$+26.0\%$	$+27.1\%$	-3.2%	-3.9%
10	$+28.5\%$	$+49.3\%$	$+146.3\%$	$+110.0\%$	-47.8%	-28.9%	$+41.2\%$	$+42.4\%$	$+64.6\%$	$+65.7\%$	-14.2%	-14.0%
PL	$-L\,(N)$		$D\,(N)$		$-L/D\,(N)$		$-L\,(N)$		$D\,(N)$		$-L/D\,(N)$	
(m)	γ-$Re_{\theta t}$	$R.\ k$-ϵ	γ-$Re_{\theta t}$	$R.\ k$-ϵ	γ-$Re_{\theta t}$	$R.\ k$-ϵ	γ-$Re_{\theta t}$	$R.\ k$-ϵ	γ-$Re_{\theta t}$	$R.\ k$-ϵ	γ-$Re_{\theta t}$	$R.\ k$-ϵ
0.18	-0.6724%	-0.6%	$+1.1\%$	$+1.6\%$	-1.8%	-2.2%	$+11.0\%$	$+11.3\%$	$+8.88\%$	$+7.9\%$	$+2.0\%$	$+3.2\%$
0.36	**931.7**	**1028.8**	**74.2**	**74.7**	**12.56**	**13.78**	**1289.6**	**1332.1**	**110.3**	**117.9**	**11.69**	**11.30**
0.54	$+1.6\%$	$+0.9\%$	-2.3%	-3.2%	$+4.0\%$	$+4.3\%$	-9.7%	-8.7%	-12.2%	-13.0%	2.8%	$+4.9\%$

Table 7: Traditional rear wing aerodynamic optimisation results. (Note the highlighted best candidate design).

Design point	MW AoA	MW PC	PL	$-L$ (N)	Δ %	D (N)	Δ %	$-L/D$	Δ %
Baseline	1	0.3	0.36	1028.8	—	74.7	—	13.78	—
1st. design point	5.5	0.27	0.62	1236.6	—	93.1	—	13.29	—
Candidate point 1	5.406	0.272	0.616	1247.0	+0.84	92.6	−0.51	13.47	+1.37
Candidate point 2	5.497	0.270	0.619	1241.7	+0.41	92.8	−0.28	13.38	+0.70
Candidate point 3	5.499	0.270	0.619	1238.2	+0.13	92.8	−0.28	13.34	+0.41

Table 8: Proposed rear wing aerodynamic optimisation results. (Note the highlighted best candidate design).

Design point	MW AoA	MW PC	PL	$-L$ (N)	Δ %	D (N)	Δ %	$-L/D$	Δ %
Baseline	1	0.3	0.36	1332.1	—	117.9	—	11.30	—
1st. design point	2.5	0.27	0.6	1234.2	—	94.83	—	13.01	—
Candidate point 1	2.717	0.25	0.55	1235.8	+0.13	92.9	−1.99	13.30	+2.17
Candidate point 2	3	0.258	0.596	1237.4	+0.26	93.5	−1.38	13.23	+1.67
Candidate point 3	2.999	0.260	0.604	1239.1	+0.40	93.5	−1.37	13.25	+1.79

ficiency, as seen in Table 6. Regarding the proposed wing vertical supports positioning, both increase (less affected flow interference region) and reduction (more lifting surface area) in the distance between them showed considerable improvements in efficiency.

4.4. Aerodynamic Optimisation

Following the parametric studies, the optimisation design variables chosen were those that most positively influenced the aerodynamic performance of the wings: the main wings (MW) profile chord (PC), main wings angle of attack (AoA) and vertical supports position (PL). To make a correct comparison between both designs, the objective function (drag minimisation) and constraint function (downforce > 1200 N) were defined similarly. Also, the baseline parameters values were changed seeking better efficiency, to fulfil the constraint defined, and to reduce the computational effort. These configurations were defined as the 1st. design point. The decisions for the 'best candidates' (candidate points) was made with objective function and wing efficiency values evaluation. The traditional and proposed design optimisation problems results are presented in Tables 7 and 8, respectively.

The traditional rear wing optimisation process took around two days of computational time to achieve convergence, as a result of 46 function evaluations to conclude 3 optimisation iterations. The NLPQL progresses towards an increase of the profile chord with decreasing the wing angle of attack. In relation to the vertical supports position, a slight decrease in the distance between them.

With respect to the proposed rear wing optimisation process, it took three days of computational time to achieve convergence, as a result of 106 function evaluations to perform 10 optimisation iterations. The optimisation progression was towards an increase in the vertical supports distance, with decrease of the main wing chord and increase of the main wing angle of attack.

4.5. Structural Parametric Studies

For the structural analyses, candidate points 1 geometries were considered, for a flow velocity of 90 m/s, as mentioned in Subsection 3.3, where the aerodynamic loads are more significant and structural behaviour would be compromised. At this flow velocity, the optimal traditional rear wing produced 4060.6 N of downforce and 301.0 N of drag, and the optimal proposed design produced 4012.3 N and 300.5 N, both with 'VI Opt.' test case (realizable k-ϵ) model application.

Table 9: Effect of material for the TRW design.

Material	Mass	U_{max}	Tsai-Hill FC
Aluminium alloy	17.971	0.85	—
ABS plastic	6.747	25.90	—
RC200T woven	7.065	2.34	0.492
HMC 300G UD	9.718	1.16	0.301

First, the traditional rear wing structural behaviour was investigated for different commonly used materials in the design of rear wings. Results are given in Table 9, where the thickness of the isotropic materials was set to 4.8 mm and for the composite materials, 16 plies at 0 deg for the HMC 300G unidirectional prepreg and RC200T woven prepreg. It is clear the advantages of CFRTP prepregs regarding the weight-to-strength ratio. In all structural analyses performed, U_{max} is the value of maximum deformation in mm, FC is the failure criterion designation, and mass is given in kg. The material chosen to be used in the designs was the

Table 10: Traditional rear wing structural optimisation results for minimisation of mass, using sets of $[(45{,}90)_n]s$ for the stacking sequence of Wing Skin/Wing Spars/Endplates.

Design point	n	Mass (kg)	Δ %	U_{max} (mm)	Δ %	Tsai-Hill FC	Δ %
1st. design point	3/3/3	5.299	—	2.50	—	0.61	—
Candidate point 1	2/2/2	3.533	−33.33	3.93	+56.93	0.87	+44.05
Candidate point 2	2/2/1	3.201	−39.58	18.39	+634.63	0.88	+44.99
Candidate point 3	2/3/1	3.298	−37.77	18.39	+634.39	0.85	+40.50

Table 11: Proposed Rear Wing structural optimisation results for minimisation of mass, using sets of $[(30{,}90)_n]s$ for the stacking sequence of MW Skin/LW Skin/MW Spars/LW Spars/Endplates.

Design Point	n	Weight (kg)	Δ %	U_{max} (mm)	Δ %	Tsai-Hill FC	Δ %
1st. design point	4/4/4/4/4	9.585	—	27.69	—	0.82	—
Candidate point 1	3/3/2/2/1	5.871	−38.75	38.49	+38.98	0.84	+2.69
Candidate point 2	3/4/2/2/1	5.960	−37.82	38.02	+37.30	0.84	+2.61
Candidate point 3	3/3/3/2/1	6.313	−34.13	37.12	+34.03	0.69	−14.91

RC200T woven [0/90] prepreg which have the lower density and smaller cured ply thickness. The structural parametric studies were carried by evaluating not only the number of plies (multiples of 4), but also the plies orientations for balanced symmetric laminates.

From the effect of the number of plies (sets of $[90_n]$) with respect to the structures mass without laminate failure prediction (Tsai-Hill and Maximum Stress criteria), this was achieved with 8 plies for the traditional design (although 12 plies have been considered as the baseline number of plies) and for the proposed one, 16 plies. Sequential cross-ply orientations of $[(90/90)_n]s$, $[(30/90)_n]s$, $[(45/90)_n]s$ and $[(60/90)_n]s$ were also evaluated. For the traditional design, more significant increase in stiffness (-21.07% U_{max}) was achieved using a $[(45/90)_3]s$ laminate set, and for the proposed design, increase in failure performance with a $[(30/90)_4]s$ set. These were the laminates defined as the baseline for the structural optimisation problems.

With respect to the structural behaviour, both designs experienced mainly bending (similar to a three-point bending problem) as seen in Fig. 9. The traditional design critical failure performance region was for the connection between the wing and supports, and for the proposed design, at the connection between the front spars (of lower wings) and supports.

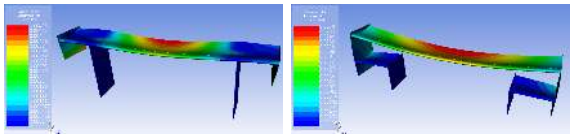

(a) TRW (10:1 scale). (b) PRW (5:1 scale).

Figure 9: Structural response of rear wings (1st. design point in Tables 10 and 11).

4.6. Structural Optimisation

The goal optimisation was to find the thinnest stacking sequence (minimum wing mass) without laminate failure, where the constraint functions were defined as $U_{max} < 0.4\ mm$ and Tsai-Hill failure criterion value < 0.9. The number of plies for the main wings, spars, and endplates were the design variables of interest. Results are given in Tables 10 and 11 for the traditional and proposed designs, respectively.

4.7. Final Results

When comparing the mesh density used in the parametric and optimisation studies (coarse), with the final analyses (fine), also the overall efficiency was improved. However, for the traditional rear wing, aerodynamic performance ($-L/D$) reduced substantially when using the fine mesh (-10.97%) and the constraint function of downforce $> 1200N$

Table 12: Rear wing designs performance comparison final results.

	$-L$ (N)	Δ %	D (N)	Δ %	$-L/D$	Δ %	W (kg)	Δ %	U_{max} (mm)	Δ %	T-H FC	Δ %
TRW (50 m/s)	1154.5	—	96.3	—	11.99	—	—	—	—	—	—	—
PRW (50 m/s)	1209.4	+4.76	88.9	−7.65	13.60	+13.44	—	—	—	—	—	—
TRW (90 m/s)	3778.9	—	309.3	—	12.22	—	3.53	—	4.38	—	0.97	—
PRW (90 m/s)	3957.5	+4.73	286.5	−7.38	13.81	+13.07	6.31	+78.75	31.72	+624.82	0.97	−0.01

was not satisfied.

Comparing the final results for the optimal rear wing designs (Table 12), with the fine mesh strategy, the proposed design proved to be aerodynamically much more efficient, by +13%. This was related to a successfully reduction of the predictable unfavourable flow interaction between the main wing and lower wings. Furthermore, as this design approach has more design variables, a larger space for changes remains, increasing its possible range of operation conditions and further improvements when compared to the traditional design. The downsides of such proposed design are associated with its structural performance. The superior surface area (+35.65%) and the considerable greater main wing deformation (7.25 times higher), resulted in a 1.79 times heavier rear wing design.

5. Conclusions

From the studies performed in this work, the MDAO process for optimal preliminary design was developed for rear wings but it can be also applied to any other automotive aerodynamic device. The use of CAE tools proved to be an efficient system to assure multidisciplinary synergy.

Mesh and turbulence modelling strategies are extremely important regarding the accuracy and reliability of the numerical solutions. If no complex three-dimensional flow behaviours are expected, the realizable k-ϵ turbulence model (with non-equilibrium wall functions) with relative coarse meshes proved to be a good trade-off regarding computational effort and solution accuracy.

If small deformations are expected, a FSI one-way coupling technique to solve the aero-structural problems has significant computational advantages in obtaining structural efficiency.

Parametric studies of the design variables leverage the optimisation computational time to obtain optimal designs by focusing on the most important or impacting variables.

References

[1] F.-K. Benra, H. Dohmen, J. Pei, S. Shuster, and B. Wan. A comparison of one-way and two-way coupling methods for numerical analysis of fluid-structure interactions. *Journal of Applied Mathematics*, 2011. Volume 2011, Article ID 853560, 16 pages.

[2] M. J. Hoffmann, R. R. Ramsay, and G. M. Gregorek. Effects of grit roughness and pitch oscillations on the NACA 4415 airfoil. Technical Report NREL/TP-442-7815, National Renewable Energy Laboratory, July 1996.

[3] J. Katz. *Race Car Aerodynamics: Designing for Speed*. Bentley Publishers, 1995.

[4] J. Kesti and S. Olsson. Fluid structure interaction analysis on the aerodynamic performance of underbody panels. Master thesis in fluid and solid mechanics, Chalmers Univerity of Technology, 2014.

[5] M. Lanfrit. Best practice guidelines for handling automotive external aerodynamics with fluent. Technical report, Fluent Deutschland GmbH, February 2005.

[6] F. R. Menter. Turbulence modeling for engineering flows. Technical report, ANSYS, Inc., 2011. A Technical Paper from ANSYS, Inc.

[7] J. N. Reddy. *Mechanics of Laminated Composite Plates and Shells - Theory and Analysis*. CRC Press, 2nd edition, 2004.

[8] A. Shedden. The design and optimisation of an aerodynamic package for an Aston Martin V8 Vantage eligible to complete in the Britcar championship. Master thesis in motorsport engineering, Oxford Brookes University, August 2010.

[9] A. Sheldon, E. Helwig, and Y. Cho. Investigation and application of multi-disciplinary optimization for automotive body-in-white development. In *8th European LS/DYNA Users Conference*, May 2011.

[10] N. P. Tedford and R. R. A. J. Martins. Benchmarking multidisciplinary design optmization algorithms. *Optimization and Engineering*, 11:159–183, 2010.

[11] J. M. Vassen, P. DeVincenzo, C. Hirsch, and B. Leonard. Strong coupling algorithm to solve fluid-structure interaction problems with a staggered approach. In *Proceedings of the 7th European Symposium on Aerothermodynamics*, pages 128–134, 2011. Brugge, Belgium.

[12] D. C. Wilcox. *Turbulence Modeling for CFD*. DCW Industries, Inc., 2th edition, 1998.